Quantum Monte Carlo Simulation Studies of the Structures of the Liquid−Vapor Interfaces of Sn and Pb

Stuart A. Rice* and Meishan Zhao

The James Franck Institute and Department of Chemistry, The University of Chicago, Chicago, Illinois, 60637

Received: May 20, 1999; In Final Form: August 3, 1999

We report the results of self-consistent quantum Monte Carlo simulations of the structure of the liquid−vapor interfaces of the tetravalent metals Sn and Pb.

I. Introduction

The liquid−vapor interface is a self-supporting region separating coexisting gaseous and liquid phases which have very different densities, hence it is a natural vehicle for the study of the properties of inhomogeneous fluids. It is now firmly established that the structure of the liquid−vapor interface of a simple fluid depends on features of the intermolecular potential which are different in dielectrics and metals.[1] In a dielectric liquid, whose potential energy is adequately represented by a sum of density-independent pair interactions, the longitudinal density profile in the liquid−vapor interface (i.e., along the normal to the interface) monotonically decreases as one passes from the bulk liquid side to the vapor side of the interface; near the triple point of the liquid the width of that profile is about 2−3 molecular diameters. In contrast, in a liquid metal the interaction between a pair of ion cores has a strong dependence on the electron density, so the pair interactions in the liquid−vapor interface depend on position along the normal to the interface. In this case the longitudinal density distribution in the liquid−vapor interface has pronounced oscillations; near the freezing point of the metal these oscillations penetrate three to four atomic diameters into the bulk liquid.[2−29] The stratification of the liquid−vapor interface of a metal can be interpreted as a signature of the strong confining force exerted on the ion cores in the interface, and the confining force can be traced to the density dependence of the volume term in the potential energy functional of the electron−ion core system.

The most useful current theoretical description of the structure of a liquid metal−vapor interface is derived from self-consistent quantum Monte Carlo simulations. The analytical basis for the simulations, as first developed by D'Evelyn and Rice[2−4] and later refined by Harris, Gryko, and Rice,[5,6] is the density functional pseudopotential representation of the properties of an inhomogeneous metal. The calculation of the nonlocal pseudopotential requires, as input, the electron density distribution in the inhomogeneous metal; this distribution is obtained from the solution to the relevant Kohn−Sham equation. The nonlocal pseudopotential of the system is then used in a Monte Carlo simulation of the system properties. Since the local electron density changes when the ion cores are moved, the pseudopotential must be recalculated after each Monte Carlo move. This procedure, when carried to convergence, generates self-consistent electron and ion core distributions for the inhomogeneous metal.

Despite the use of a sophisticated nonlocal representation of the atomic interactions in the inhomogeneous liquid, it must be recognized that the analysis outlined above contains numerous approximations, e.g., in the treatment of the exchange and kinetic energies, and in the neglect of a possible metal-to-nonmetal transition in the interface. Moreover, even the best pseudopotentials rarely yield an accurate binding energy for the liquid metal. Indeed, it is common practice to modify a calculated pseudopotential by addition of terms representing the core−core repulsion and the core−core dispersion interaction, parameterized to yield the correct liquid binding energy and vapor pressure. It is, therefore, necessary to test the adequacy of theoretical predictions of the liquid−vapor interface structure that are based on use of a pseudopotential representation for a variety of metals with different valences and with different ion core states. Wherever possible those tests should be based on a comparison of the predicted and observed longitudinal density distribution in the liquid−vapor interface. It is also necessary that there be good agreement between the predicted and observed pair correlation functions of the bulk liquid metal.

To date, self-consistent quantum Monte Carlo simulations of the liquid−vapor interfaces of some simple monovalent metals[2−6,14] (Na and Cs), some divalent metals[7,15] (Hg and Mg), and some trivalent metals[8,10] (Ga, Al, In, and Tl) have been reported. In all of these cases there is very good agreement between the predicted and observed pair correlation functions of the bulk liquid metal. And, for the systems for which experimental data exist, Ga, Hg, and In, there is very good agreement between the predicted and experimentally inferred longitudinal density distributions in the liquid−vapor interfaces.[22,24,25,28]

In this paper we report the results of self-consistent quantum Monte Carlo simulations of the liquid−vapor interfaces of the tetravalent metals Sn and Pb. These calculations were undertaken to test the adequacy of the pseudopotential based theory for tetravalent metals, and to provide the information necessary to begin studies of component segregation, longitudinal structure and transverse structure in the liquid−vapor interfaces of alloys in which Sn and/or Pb are component species.

II. Theoretical Background

As indicated in the Introduction, our analysis of the structure of an inhomogeneous liquid metal is based on a pseudopotential representation of the Hamiltonian.[8] The derivation of this representation is described elsewhere[5]; the result is

$$\mathbf{H} = \sum_{i=1}^{N} \frac{\mathbf{p}_i^{\,2}}{2m} + \sum_{i=1}^{N}\sum_{j<i}^{N} \phi_{\mathrm{eff}}(|\mathbf{R}_i - \mathbf{R}_j|;n_{\mathrm{e}}(\mathbf{r})) + U_0[\rho_0(\mathbf{r}), n_{\mathrm{e}}(\mathbf{r})] \quad (1)$$

10.1021/jp991669z CCC: $18.00
Published on Web 09/03/1999

where $\boldsymbol{p}_i$ is the momentum of the ith atom with mass m, $\phi_{\text{eff}}(|\mathbf{R}_i - \mathbf{R}_j|;n_e(\mathbf{r}))$ is the effective pair potential between ions i and j, $R = |\mathbf{R}_i - \mathbf{R}_j|$ is the separation of ions i and j, and $\rho_0(\mathbf{r})$ and $n_e(\mathbf{r})$ are reference jellium and electron densities, respectively. The functional $U_0[\rho_0(\mathbf{r}), n_e(\mathbf{r})]$ is a structure-independent contribution to the energy which is, however, dependent on the electron and jellium densities. Note that we use atomic units for all physical quantities in the following discussion unless specified otherwise.

We have used the simplest local density approximation to the ion−ion effective pair potential, namely,

$$\phi_{\text{eff}} = \phi_{\text{H}}(R; {}^1/_2[n_e(\mathbf{R}_i) + n_e(\mathbf{R}_j)]) \tag{2}$$

In a homogeneous fluid with electronic density $n_e(\mathbf{r})$ this effective pair potential is given by

$$\phi_{\text{H}}(R) = \frac{(z^*)^2}{R}\left\{1 - \frac{2}{\pi}\int_0^\infty \frac{F_{\text{N}}(q)\,\text{in}(qR)}{q}\,\text{d}q\right\} + \phi_{\text{BM}}(R) + \phi_{\text{vdw}}(R) \tag{3}$$

The first term in eq 3 is due to the direct Coulomb repulsion between ions with effective valence charge z^*, where $(z^*)^2 = Z^2 - \bar{Z}^2$ with Z the true valence charge and $\bar{Z}$ the depletion hole charge that originates from the required orthogonality of the valence and core electron wave functions. The second term in eq 3 is an indirect interaction mediated by the conduction electrons (called the band structure energy). This contribution to the effective pair potential tends to offset the effect of the strong Coulomb repulsion between ion cores and thus lowers the energy of the system. Finally, $\phi_{\text{BM}}(R)$ is the Born−Mayer core−core repulsion potential[30]

$$\phi_{\text{BM}}(R) = A_{\text{BM}}\text{e}^{-B_{\text{BM}}R} \tag{4}$$

where A_{BM} and B_{BM} are parameters and $\phi_{\text{vdw}}(R)$ is the van der Waals dispersion interaction between the ion cores. In general, both $\phi_{\text{BM}}(R)$ and $\phi_{\text{vdw}}(R)$ are much smaller than the other contributions to the energy.

The band structure energy term in eq 3 contains the normalized energy wavenumber characteristic function $F_{\text{N}}(q)$. Shaw[31,32] has shown that

$$F_{\text{N}}(q) = \frac{\Omega^2 q^4}{16\pi^2(z^*)^2}\left\{\frac{[1-\epsilon(q)]\,(\upsilon_1+\upsilon_2)^2}{\epsilon(q)} + 2g(q)\,(\upsilon_1 + \upsilon_2) + \epsilon(q)g(q)^2 + h(q)\right\} \tag{5}$$

where $\Omega = (\rho_{\text{bulk}})^{-1}$ is the volume per atom, ρ_{bulk} is the bulk liquid density, and ϵ(q) is the wavenumber-dependent Hartree dielectric function

$$\epsilon(q) = 1 + \frac{1}{2\pi k_{\text{F}}\eta^2}\left[1 + \frac{1-\eta^2}{2\eta}\ln\left(\left|\frac{1+\eta}{1-\eta}\right|\right)\right] \tag{6}$$

where k_{F} is the Fermi wavenumber and $\eta = q/2k_{\text{F}}$. The terms denoted $g(q)$ and $h(q)$ are a nonlocal screening function defined by

$$g(q) = \frac{4}{\pi^2 q^2 \epsilon(q)}\int_{k\le k_{\text{F}}} \frac{f(\mathbf{k},\mathbf{q})}{k^2 - |\mathbf{k}+\mathbf{q}|^2}\,\text{d}\mathbf{k} \tag{7}$$

and a nonlocal bare pseudopotential contribution which, to second order, has the form

$$h(q) = \frac{4}{\pi^2 q^2}\int_{k\le k_{\text{F}}} \frac{|f(\mathbf{k},\mathbf{q})|^2}{k^2 - |\mathbf{k}+\mathbf{q}|^2}\,\text{d}\mathbf{k} \tag{8}$$

with

$$f(\mathbf{k},\mathbf{q}) = -N\langle \mathbf{k}+\mathbf{q}|V_{\text{ps}}^{\text{ion}}|\mathbf{k}\rangle \tag{9}$$

In eq 9, $V_{\text{ps}}^{\text{ion}}$ is the nonlocal bare pseudopotential. The local potential contributions υ_1 and υ_2, arising from the valence charge Z and the depletion hole charge $\bar{Z}$, respectively, are given by

$$\upsilon_1 = -\frac{4\pi}{\Omega q^2}Z \tag{10}$$

$$\upsilon_2 = -\frac{4\pi}{\Omega q^2}\bar{Z} \tag{11}$$

The structure-independent energy $U_0[\rho_0(\mathbf{r}),n_e(\mathbf{r})]$ is a functional of the reference jellium density and of the electronic density. Using the local density approximation, it has the form

$$U_0[\rho_0(\mathbf{r}), n_e(\mathbf{r})] = \frac{3(3\pi^2)^{2/3}\sigma}{10}\int_0^\infty [n_e(\mathbf{r})]^{5/3}\,\text{dz} + \frac{\sigma}{72}\int_0^\infty \frac{|\nabla^2 n_e(\mathbf{r})|}{n_e(\mathbf{r})}\,\text{dz} + \frac{\sigma}{540\,(3\pi^2)^{2/3}}\int_0^\infty \text{dz}\,[n_e(\mathbf{r})]^{2/3}\times\left[\left(\frac{\nabla^2 n_e(\mathbf{r})}{n_e(\mathbf{r})}\right)^2 - \frac{9}{8}\left(\frac{\nabla^2 n_e(\mathbf{r})}{n_e(\mathbf{r})}\right)\left(\frac{\nabla n_e(\mathbf{r})}{n_e(\mathbf{r})}\right)^2 + \frac{1}{3}\left(\frac{\nabla n_e(\mathbf{r})}{n_e(\mathbf{r})}\right)^4\right]^2 - 2\pi\sigma\int_0^\infty \text{dz}\int_0^\infty \text{dz}'\,[\rho_0(z)\,\rho_0(z') - n_e(z)\,n_e(z')]|z-z'| + 2\sigma\int_0^\infty n_e(z)\,\epsilon_{\text{xc}}[n_e(z)]\,\text{dz} + 2\sigma\int_0^\infty \rho_0(z)\,\epsilon_{\text{ps}}[n_e(z)]\,\text{dz} \tag{12}$$

The first three terms of eq 12 are, respectively the Fermi−Thomas uniform density contribution to the kinetic energy of the electrons in a liquid metal with surface area σ, the von Weizacker first density correction to the kinetic energy of the inhomogeneous electron gas,[33] and the Kirzhnits second-order gradient correction to the kinetic energy of the inhomogeneous electron gas.[34] The fourth term is the electrostatic energy of the system arising from the difference between the electron and ion density distributions in the liquid−vapor interface, and the fifth term is the exchange-correlation contribution to the energy calculated using the homogeneous electron gas as proposed by Vosko, Wilk, and Nusair,[35] with the density gradient correction proposed by Langreth and Mehl.[36] The last term in eq 12 is the electron−ion pseudopotential contribution to the electronic energy, with $\epsilon_{\text{ps}}[n_e(z)]$ the ionic pseudopotential (which is a function of the electron density distribution).

The pseudopotential contribution to the structure-independent energy is contained in $\epsilon_{\text{ps}}[n_e(z)]$, which has the form

$$\epsilon_{\text{ps}} = \frac{3}{k_{\text{F}}^3}\int_0^{k_{\text{F}}} f(q,q)q^2\,\text{d}q - \frac{1}{\pi}\,\text{d}q\{\bar{Z}^2|M(q)|^2 - (z^*)^2 F_{\text{N}}(q)\} - \frac{2\pi(z^*)^2}{\Omega}\lim_{q\to 0}\frac{1-F_{\text{N}}(q)}{q^2} + \left(\frac{\alpha}{r_s} + \frac{\beta}{r_s^2}\right) \tag{13}$$

where $f(q, q')$ is the diagonal matrix element of the Fourier transform of the nonlocal bare electron−ion pseudopotential,

$M_i(q)$ is the Fourier transform of the depletion hole distribution, and r_s is defined by

$$\frac{1}{n_{\mathrm{e,bulk}}} = \frac{4\pi}{3} r_s^3 \tag{14}$$

where $n_{\mathrm{e,bulk}}$ is the electron density of the bulk liquid. The terms (α/r_s) and (β/r_s^2) are semiempirical corrections. The parameters α and β were determined by imposing the requirement that the calculated and observed pressure and heat of vaporization of the liquid metal agree with experimental values at the liquid density.

In our calculations we employed the nonlocal energy-independent model pseudopotential proposed by Woo, Wang, and Matsuura[37]

$$V_{\mathrm{ps}}^{\mathrm{ion}}(r) = \sum_l \{\bar{V}_l(r) + [V_{1l}(r) - \bar{V}_l(r)]|R_{1l}\rangle \langle R_{1l}|\}\ |l\rangle \langle l| \tag{15}$$

$$V_{1l}(r) = \begin{cases} -B_{1l} + Z_{l/r}, & r \le R_l \\ Z_{l/r}, & r > R_l \end{cases} \tag{16}$$

In eq 15, $|R_{1l}\rangle$ is the radial part of the wave function for state $|1l\rangle$, and $|l\rangle$ is a simple projection onto the state with angular momentum l, while $\bar{V}_l(r)$ is a pseudopotential average over all states other than the first valence state with a given angular momentum l. It has the same form as $V_{1l}(r)$ except that the parameter B_{1l} is replaced by $\bar{B}_{1l}$. The potential parameters B_{1l}, Z_l, R_l are are usually determined by a pseudo-eigenfunction expansion and perturbation theory. The state $|1l\rangle$ is separated into radial and angular parts, such that

$$\langle \mathbf{x}|1l\rangle = N \frac{1}{r} y_{1l}(r) Y_{lm}(\theta, \phi) \tag{17}$$

where N is a normalization constant, $Y_{lm}(\theta, \phi)$ is a spherical harmonic function, and $y_{1l}(r)$ is the radial wave function given by

$$y_{1l}(r) = \begin{cases} M_{\nu,l+1/2}(2\lambda r), & r \le R_l \\ W_{\nu 0,l+1/2}(2\lambda_0 r), & \mathrm{r} > R_l \end{cases} \tag{18}$$

where $M_{\nu,l+1/2}(2\lambda r)$ and $W_{\nu_0,l+1/2}(2\lambda_0 r)$ are respectively the regular and irregular Whittacker functions.[38] The parameters of the Whittacker functions are

$$\lambda_0 = \sqrt{-2E_{1l}} \tag{19}$$

$$\lambda = \sqrt{-2(E_{1l} + B_{1l})} \tag{20}$$

$$\nu_0 = \frac{Z_l}{\sqrt{-2E_{1l}}}, \tag{21}$$

$$\nu = -\frac{Z_l}{\sqrt{-2(E_{1l} + B_{1l})}} \tag{22}$$

with E_{1l} the spectroscopic term energy of state $|1l\rangle$. The values of the potential parameters we have used for Sn and Pb are displayed in Table 1. We show in Figure 1 the effective ion−ion pair interaction potential for liquid Sn with density 0.0350 atoms/Å^3, and in Figure 2 the effective ion−ion pair interaction potential for liquid Pb with density 0.0310 atoms/Å^3.

The reference atomic density profile in the pseudoatom Hamiltonian is taken to be the jellium profile. Our simulations were carried out for a slab of ions with two surfaces perpendicular to the z axis and the jellium density distribution

$$\rho(z,z_0,\beta) = \rho_{\mathrm{bulk}}\left[1 + \exp\left(\frac{|z| - z_0}{\beta'}\right)\right]^{-1} \tag{23}$$

where z_0 is the position of the Gibbs dividing surface and β' measures the width of the inhomogeneous region of the profile. This distribution is normalized by setting $\rho_{\mathrm{bulk}} = N/2\sigma z_0$, where N is the total number of atoms in the slab and σ is the area of the slab. The parameters z_0 and β' are varied to obtain the best fit to the instantaneous ionic configuration.

Given the reference profile, the electron density distribution is obtained by a self-consistent solution to the Kohn−Sham equation[39,40]

$$\left[-\frac{\hbar}{2m}\nabla^2 + V_{\mathrm{eff}}(\mathbf{r})\right]\psi_n(z) = E_n\psi_n(\mathbf{r}) \tag{24}$$

where $V_{\mathrm{eff}}(\mathbf{r})$ is an effective potential that includes the electron−

TABLE 1: Ionic Pseudopotential Parameters (in atomic units)[a]

metal	l	E_{1l}	R_l	B_{1l}	$r_{\max}$
Sn	0	1.120 927	0.911 00	4.430 40	35.0
	1	0.526 250	1.474 50	2.712 00	45.0
	2	0.269 887	5.332 00	4.819 60	55.0
Pb	0	1.554 863	2.007 23	1.997 71	35.0
	1	1.206 899	1.888 94	2.124 80	45.0
	2	0.714 190	2.662 49	1.511 53	55.0

[a] $r_{\max}$ is the maximum value of r in the radial wave function.

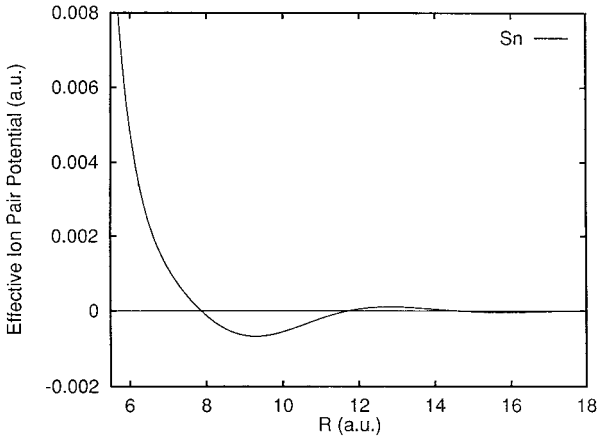

Figure 1. Effective ion−ion pair potential in liquid Sn with density 0.0350 atoms/Å^3.

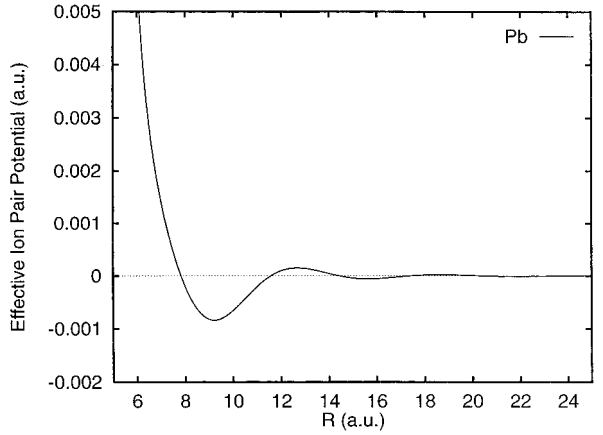

Figure 2. Effective ion−ion pair potential in liquid Pb with density 0.0310 atoms/Å^3.

jellium background pseudopotential interaction $V_{ps}(\mathbf{r})$, the exchange−correlation potential $V_{xc}(\mathbf{r})$, and the electrostatic potential

$$V_{eff}(\mathbf{r}) = V_{ps}(\mathbf{r}) + V_{xc}(\mathbf{r}) + \int d\mathbf{r} \frac{n_e(\mathbf{r})}{|\mathbf{r} - \mathbf{r}'|} \quad (25)$$

The exchange-correlation potential $V_{xc}(\mathbf{r})$ is defined as the derivative

$$V_{xc}(\mathbf{r}) = \frac{\delta E_{xc}[n_e(\mathbf{r})]}{\delta n_e} \quad (26)$$

where $E_{xc}[n_e(\mathbf{r})]$ is the exchange and correlation energy functional, and the electron number density is calculated from

$$n_e(\mathbf{r}) = \sum_{n=1}^{\infty} f_n |\psi_v(\mathbf{r})|^2 \quad (27)$$

with f_v the electron ocupation number in state $|\psi_v(\mathbf{r})\rangle$.

The jellium ion density distributions in the x and y directions are uniform, hence so must be the corresponding electron density distributions. The electronic wave function $\psi_n(\mathbf{r})$ can then be written as

$$\psi_n(\mathbf{r}) = e^{i(k_x x + k_y y)} \phi_n(z) \quad (28)$$

where k_x and k_y are the wavenumbers in the x and y directions, respectively. Then the electron density $n_e(\mathbf{r}) \equiv n_e(z)$ is a function of z only, which can be obtained by solving the one-dimensional Kohn−Sham equation

$$\left[-\frac{\hbar}{2m} \frac{d^2}{dz^2} + V_{eff}(z; n_e(z)) \right] \phi_n(z) = \epsilon_n \phi_v(z) \quad (29)$$

We find

$$E_n = \frac{\hbar^2}{2m_e} (k_x^2 + k_y^2) + \epsilon_n, \quad n = 1, 2, ... \quad (30)$$

and the electron density profile

$$n_e(z) = \sum_{v=1}^{\infty} f_v |\phi_v(z)|^2 \quad (31)$$

from which we construct, in turn, the electron density dependent potential $V_{eff}(z; n_e(z))$, and again solve the one-dimensional Kohn−Sham equation. This procedure is repeated until a converged self-consistent solution is obtained.

III. Simulation Method and Results

A. Simulation Procedure. We have carried out simulations of liquid Sn at temperatures $T = 573$, 973, and 1173 K. Since the density of Sn only changes from 0.0350 to 0.0340 atoms/Å^3 over this temperature range, we have carried out all of our simulations at the fixed density 0.0350 atoms/Å^3. We have also carried out simulations of liquid Pb at temperatures T = 613, 823, 1023, and 1173 K for the corresponding equilibrium densities 0.0310, 0.302, 0.0295, and 0.0237 atoms/Å^3, respectively. As described earlier,[2−15] an assumed initial jellium distribution is used to generate an electronic density distribution from which the ion−electron pseudopotential and effective ion−ion interaction potentials are calculated. These initial jellium distributions are then used in a Monte Carlo simulation of the inhomogeneous liquid−vapor system. Since each Monte Carlo step changes the ion distribution, it also changes the electronic density distribution, and hence the ion−electron pseudopotential and the effective ion−ion interaction; this effect is particularly important in the inhomonegenous liquid−vapor transition zone. Accordingly, when the ion distribution is changed, the electron distribution is recalculated, to be consistent with the new ion distribution; this procedure is continued until the Monte Carlo simulation converges.

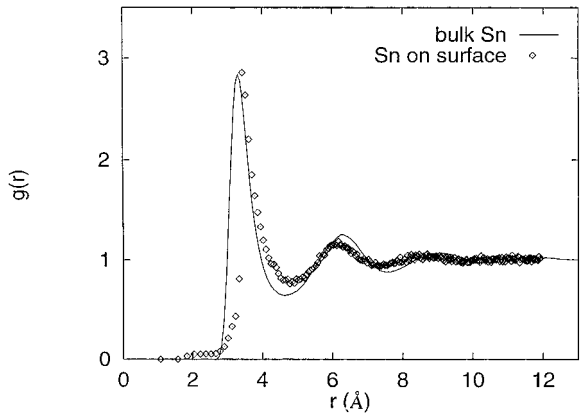

Figure 3. Comparison of the bulk liquid pair correlation function and the transverse pair correlation function in the liquid−vapor interface of Sn with density 0.0350 atoms/Å^3 at $T = 573$ K.

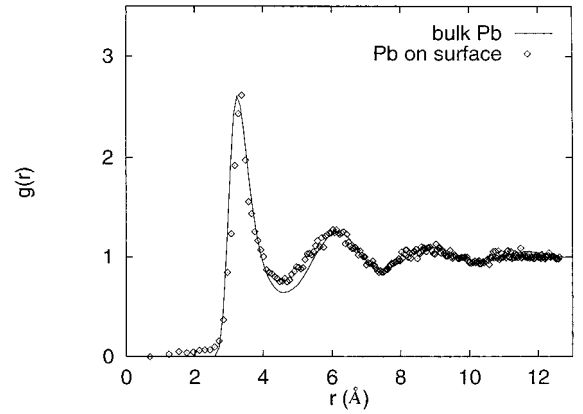

Figure 4. Comparison of the bulk liquid pair correlation function and the transverse pair correlation function in the liquid−vapor interface of Pb with density 0.0295 atoms/Å^3 at $T = 1023$ K.

The most primitive way of carrying out the program is to repeat the calculations of the effective ion−ion interaction for every move of the ions in the Monte Carlo simulation procedure. In our simulations we have adopted a more efficient computational strategy and data management scheme. Prior to starting the simulation we compute and tabulate the effective ion−ion interaction potential energies for a series of electron densities ranging from somewhat below to somewhat above the bulk density of liquid metal. During the simulation the interaction between a particular pair of ions is obtained from a rational functional interpolation for the given electron density using the precalculated data bank.

The model system for the simulations consisted of a slab of 1000 ions. The dimensions of the simulation slab were $L_0 \times L_0 \times 2L_0$ in the (x, y, z) directions, so that the area of each liquid−vapor interface is $\sigma = L_0^2$. The slab contains two free surfaces in the positive z and negative z directions (normal to the two liquid−vapor interfaces) and periodic boundary conditions in the x and y directions. In fact, periodic boundary conditions were also applied in the z direction, but at distances so far from

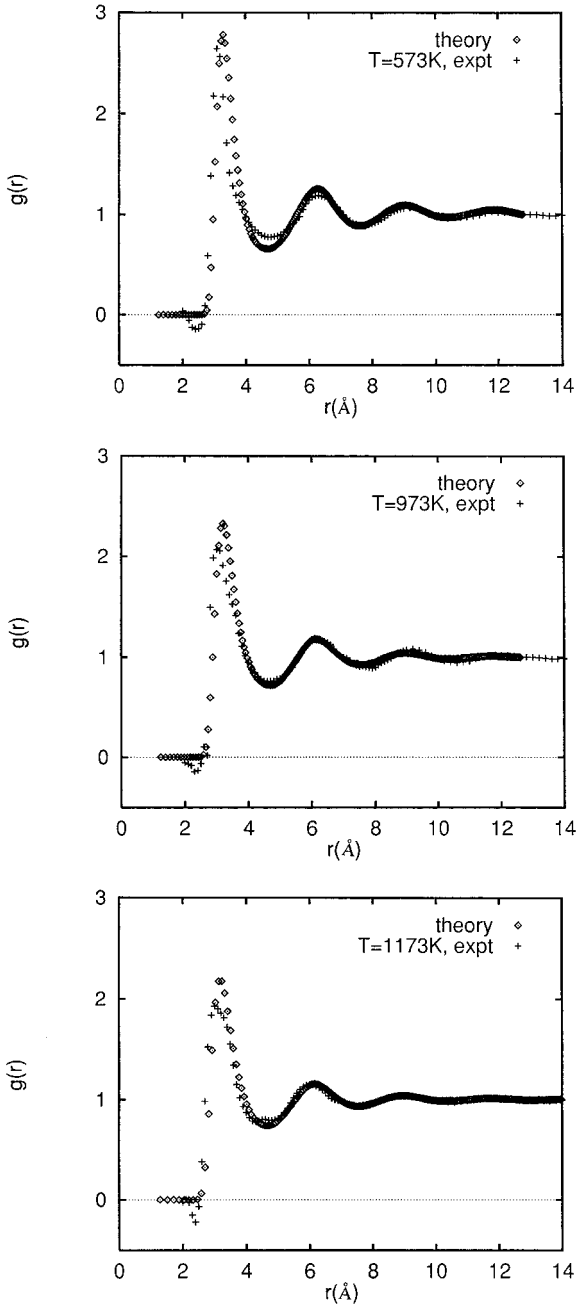

Figure 5. Comparison of the simulated and experimentally determined pair correlation functions of bulk liquid Sn at (a, top) $T = 573$ K, (b, middle) $T = 973$ K, (c, bottom) $T = 1173$ K. Experimental data from ref 41.

the liquid−vapor interfaces that the description of those interfaces as free is valid. The size of the slab L_0 was chosen such that the average density of ions in the slab matched the density of the binary alloy at the simulation temperature. The center of mass of the simulation system was located at the origin of the coordinates ($x = 0$, $y = 0$, $z = 0$). The initial ion configuration was generated by placing the particles within the boundaries of the slab, subject to the constraint that no ion−ion separation was less than the ionic diameter.

The simulations were carried out using the Metropolis scheme and a force bias Monte Carlo algorithm to eliminate the overlaps between ion cores. The trial configurations were generated by randomly displacing a selected ion; the magnitude of the ionic displacement was chosen to lead to convergence to equilibrium with a reasonable overall acceptance ratio for the trial configurations.

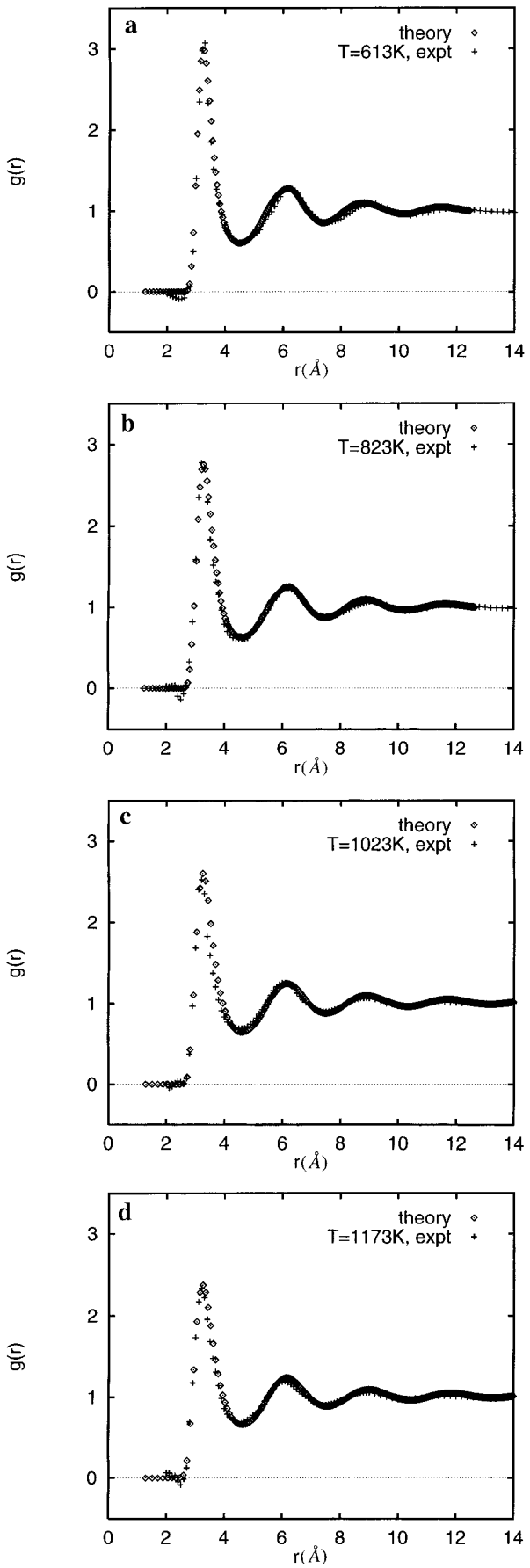

Figure 6. Comparison of the simulated and experimentally determined pair correlation functions of bulk liquid Pb at (a) $T = 613$ K, (b) $T = 823$ K, (c) $T = 1023$ K, (d) $T = 1173$ K. Experimental data from ref 41.

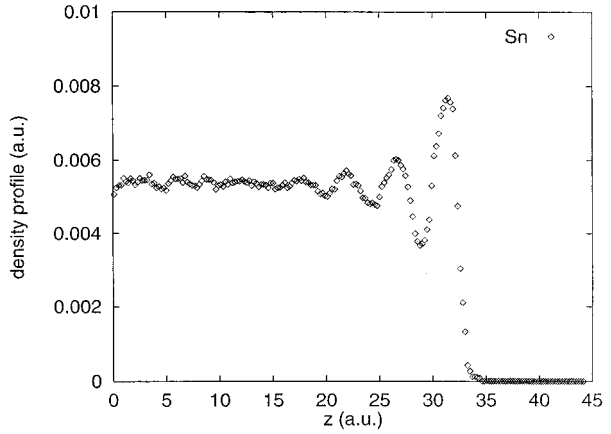

Figure 7. Longitudinal density profile of the liquid−vapor interface of Sn at $T = 973$ K with density 0.0350 atoms/Å^3.

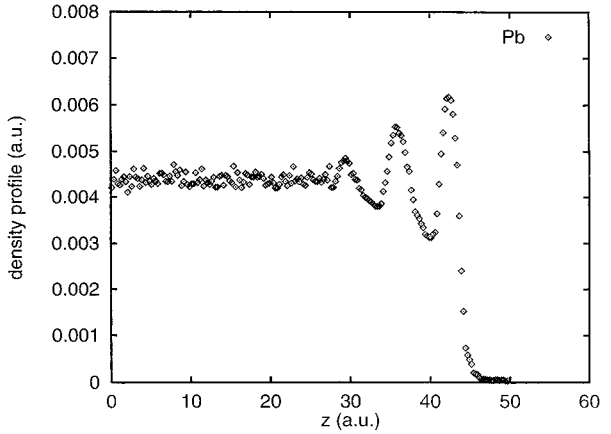

Figure 8. Longitudinal density profile of the liquid−vapor interface of Pb at $T = 1023$ K with density 0.0295 atoms/Å^3.

B. Pair Correlation Functions in the Interface and in the Bulk Liquid. The structure of the liquid−vapor interface is conveniently characterized by the transverse (in-plane) pair correlation function and the longitudinal density distribution. The transverse pair correlation function, which was calculated from a histogram of the separations of all pair of particles in a thin slice of the interfacial region, is given by

$$g(r) = \frac{2V_T N(r,\Delta r)}{V_s N_T^2} \tag{32}$$

where N_T is the total number of particles in the slice, $N(r,\Delta r)$ is the average number of pairs of particles between and in the slice, V_T is the total volume of all the particles in the slice, and V_s is the average volume of the intersection of the spherical shell between r and $(r + \Delta r)$ of the thin slice.

We show in Figure 3 the transverse pair correlation function in the liquid−vapor interface of Sn when $T = 573$ K, and in Figure 4 that of Pb when $T = 1023$ K. In each case the pair correlation function in the interface is compared with the pair correlation function of the bulk liquid at the same temperature (see below). We note that for Pb these functions are very nearly the same. There is a very small difference between the positions of the first peaks (4%) and a small difference in the depth of the trough between the first and second peaks. For Sn, in addition to the shift of the first peaks, there is a very small difference (3.4%) in the positions of the second peaks and the first peak of the transverse pair correlation function in the liquid−vapor interface is narrower than that of the pair correlation function in the bulk liquid.

We have also calculated the bulk liquid pair correlation functions for *Sn* and *Pb* at the temperatures and densities cited above. The results of these calculations are displayed in Figures 5 and 6, along with the experimentally determined pair correlation functions[41] at the same temperatures. Clearly, the simulated and experimentally determined pair correlation functions for liquid Sn are in reasonable agreement, although at $T = 573$ K the first valley of the simulated pair correlation function is deeper than that observed. The simulated and experimentally determined bulk liquid pair correlation functions for Pb are in nearly perfect agreement at all of the temperatures considered.

C. The Longitudinal Density Distribution in the Interface. The longitudinal density distribution of the ions was obtained from a histogram of the distance between a particle and the center of the mass of the slab; the density profiles in the $\pm z$ directions were averaged to obtain the reported density distribution. We show in Figure 7 the longitudinal density profile in the liquid−vapor interface of Sn when $T = 973$ K and the bulk liquid density is 0.0350 atoms/Å^3, and in Figure 8 that of Pb when $T = 1023$ K and the bulk liquid density is 0.0295 atoms/Å^3. As for the other liquid metal−vapor interfaces we have studied, these longitudinal density distributions show pronounced stratification with an overall penetration into the bulk liquid of the order of four atomic diameters and a separation between strata of an atomic diameter.

Acknowledgment. This work has been supported by a grant from the National Science Foundation.

References and Notes

(1) Rice, S. A. *J. Non-Cryst. Solids* **1996**, *205−207*, 755.
(2) D'Evelyn, M. P.; Rice, S. A. *Phys. Rev. Lett.* **1981**, *47*, 1844.
(3) D'Evelyn, M. P.; Rice, S. A. *J. Chem. Phys.* **1983**, *78*, 5081.
(4) D'Evelyn, M. P.; Rice, S. A. *J. Chem. Phys.* **1983**, *78*, 5225.
(5) Harris, J. G.; Gryko, J.; Rice, S. A. *J. Chem. Phys.* **1987**, *87*, 3069.
(6) Harris, J. G.; Gryko, J.; Rice, S. A. *J. Stat. Phys.* **1987**, *48*, 1109.
(7) Gomez, A.; Rice, S. A. *J. Chem. Phys.* **1994**, *101*, 8094.
(8) Zhao, M.; Chekmarev, D.; Cai, Z.; Rice, S. A. *Phys. Rev. E* **1997**, *56*, 7033.
(9) Zhao, M.; Chekmarev, D.; Rice, S. A. *J. Chem. Phys.* **1998**, *108*, 5055.
(10) Zhao, M.; Chekmarev, D.; Rice, S. A. *J. Chem. Phys.* **1998**, *109*, 1959.
(11) Zhao, M.; Rice, S. A. *J. Chem. Phys.* **1999**, *111*, 2181.
(12) Rice, S. A.; Zhao, M. *Phys. Rev. B* **1998**, *57*, 13501.
(13) Rice, S. A.; Zhao, M.; Chekmarev, D. *Proc. MRS* **1998**, *492*, 3.
(14) Chekmarev, D.; Zhao, M.; Rice, S. A. *J. Chem. Phys.* **1998**, *109*, 768.
(15) Chekmarev, D.; Zhao, M.; Rice, S. A. *Phys. Rev. E* **1999**, *59*, 479.
(16) Lei, N.; Huang, Z.; Rice, S. A. *J. Chem. Phys.* **1996**, *104*, 4802.
(17) Lei, N.; Huang, Z.; Rice, S. A.; Grayce, C. *J. Chem. Phys.* **1996**, *105*, 9615.
(18) Lei, N.; Huang, Z.; Rice, S. A. *J. Chem. Phys.* **1997**, *107*, 4051.
(19) Flom, E. B.; Li, M.; Acero, A.; Maskil, N.; Rice, S. A. *Science* **1993**, *260*, 332.
(20) Thomas, B. N.; Barton, S. W.; Novak, F.; Rice, S. A. *J. Chem. Phys.* **1987**, *86*, 1036.
(21) Flom, E. B.; Cai, Z.; Acero, A.; Lin, B.; Maskil, N.; Liu, L.; Rice, S. A. *J. Chem. Phys.* **1992**, *96*, 4743.
(22) Regan, M. J.; Kawamoto, E. H.; Lee, S.; Pershan, P. S.; Maskil, N.; Deutsch, M.; Magnussen, O. M.; Ocko, B. M. *Phys. Rev. Lett.* **1995**, *75*, 2498.
(23) Magnussen, O. M.; Ocko, B. M.; Regan, M. J.; Penanen, K.; Pershan, P. S.; Deutsch, M. *Phys. Rev. Lett.* **1995**, *74*, 4444.
(24) Regan, M. J.; Pershan, P. S.; Magnussen, O. M.; Ocko, B. M.; Deutsch, M.; Berman, L. E. *Phys. Rev. B* **1996**, *54*, 9730.
(25) Regan, M. J.; Pershan, P. S.; Magnussen, O. M.; Ocko, B. M.; Deutsch, M.; Berman, L. E. *Phys. Rev. B* **1997**, *55*, 15874.
(26) Regan, M. J.; Tostmann, H. C.; Pershan, P. S.; Magnussen, O. M.; DiMasi, E.; Ocko, B. M.; Deutsch, M. *Phys. Rev. B* **1997**, *55*, 10786.
(27) Tostmann, H.; DiMasi, E.; Pershan, P. S.; Ocko, B. M.; Shpyrko, O. G.; Deutsch, M. *Phys. Rev. B* **1999**, *59*, 783.

(28) DiMasi, E.; Tostmann, H.; Ocko, B. M.; Pershan, P. S.; Deutsch, M. *Phys. Rev. B* **1998**, *58*, R13419.
(29) Fukuto, M.; Heilmann, R. K.; Pershan, P. S.; Griffiths, J. A.; Yu, S. M.; Tirrell, D. A. *Phys. Rev. Lett.* **1998**, *81*, 3455.
(30) Gilbert, T. L. *J. Chem. Phys.* **1968**, *49*, 2640.
(31) Shaw, R. W., Jr. *Phys. Rev.* **1968**, *174*, 769.
(32) Shaw, R. W., Jr. *J. Phys. C* **1969**, *2*, 2335.
(33) March, N. H. *Adv. Phys.* **1957**, *6*, 1.
(34) Kirzhnits, D. A. *Sov. Phys. JETP* **1957**, *5*, 64.
(35) Vosko, S. H.; Wilk, L.; Nusair, M. *Can. J. Phys.* **1980**, *58*, 1200.
(36) Langreth, D. C.; Mehl, M. J. *Phys. Rev. B* **1983**, *8*, 1809.
(37) Woo, C. H.; Wang, S.; Matsuura, M. *J. Phys. F* **1975**, *5*, 1836.
(38) Whittacker functions.
(39) Hohenberg, P.; Kohn, W. *Phys. Rev. B* **1964**, *136*, 864.
(40) Kohn, W.; Sham, L. J. *Phys. Rev. A* **1965**, *140*, 1133.
(41) Waseda, Y. *The Structure of Non-Crystalline Materials: Liquids and Amorphous Solids*; McGraw-Hill: New York, 1980.